Geophysical Research Letters

RESEARCH LETTER
10.1029/2018GL081404

Lateral Motion of Mantle Plumes in 3-D Geodynamic Models

Mingming Li[1] **and Shijie Zhong**[2]

[1]School of Earth and Space Exploration, Arizona State University, Tempe, AZ, USA, [2]Department of Physics, University of Colorado Boulder, Boulder, CO, USA

Key Points:
- Greater than 90% plumes move laterally with a speed of 0-20 mm/year, and ~10-20% plumes are relatively fixed with a lateral motion of <5 mm/year
- The speeds of the lateral motions of plumes beneath the Pacific plate are statistically similar to those beneath the Indo-Atlantic plates
- The number, location, and lateral motion of individual plumes in convection models depend on the model parameters

Supporting Information:
- Supporting Information S1

Correspondence to:
M. Li,
mingming.li@asu.edu

Citation:
Li, M., & Zhong, S. (2019). Lateral motion of mantle plumes in 3-D geodynamic models. *Geophysical Research Letters*, *46*. https://doi.org/10.1029/2018GL081404

Received 21 NOV 2018
Accepted 30 APR 2019
Accepted article online 3 MAY 2019

Abstract It has been proposed that hot spot tracks are caused by moving rigid plates above relatively stationary hot spots. However, the fixity of hot spots remains under debate. Here, we perform 3-D very high resolution (<25 km laterally) global mantle convection models with realistic convection vigor to investigate the lateral motion of mantle plumes. We find that the lateral motion of plumes beneath the Pacific plate is statistically similar to that beneath the Indo-Atlantic plates. In the past 80 Ma, the majority (>90%) of plumes move laterally with an average speed of 0–20 mm/year under the no-net-rotation reference frame, and there are a small portion (~10–20%) of plumes whose lateral motion is less than 5 mm/year. The geodynamic modeling results are statistically in a good agreement with the hot spot motions in the last 5 Ma estimated from observation-based kinematic models. Our results suggest a small-to-moderate (0–20 mm/year) lateral motion of most plume-induced hot spots.

Plain Language Summary The intraplate volcanic islands on the Earth's surface often form progressively aged hot spot tracks. The hot spot tracks have been proposed to be caused by moving rigid plates above relatively stationary plumes. However, it remains unclear how fast mantle plumes move laterally. Here, very high resolution 3-D global mantle convection models are performed to quantify the lateral motions of all long-lived plumes. The models show that while the number, location, and lateral motion of individual plumes are rather model dependent, the majority (>90%) of plumes move laterally at a speed of 0–20 mm/year with only a small portion (~10–20%) of plumes being relatively stationary with a lateral motion less than 5 mm/year. The lateral motions of Pacific plumes and Indo-Atlantic plumes are statistically similar. Importantly, the results of plume motions are statistically in an excellent agreement with the motions of observed hot spots. The results have important implications for understanding the formation of hot spot tracks and the dynamics of mantle plumes.

1. Introduction

The intraplate volcanic islands on the Earth's surface often form progressively aged hot spot tracks. It has been shown that hot spot tracks can be produced by moving rigid plates above fixed hot spots (Morgan, 1972; Wilson, 1963). The relatively fixed hot spots provide a reference frame in which absolute plate motion is reconstructed (e.g., Duncan, 1981). However, the fixity of hot spots remains under debate (Duncan, 1981; Duncan & Richards, 1991; Gordon & Cape, 1981; Hassan et al., 2016; Molnar & Stock, 1987; Morgan, 1983; Morgan & Morgan, 2007; Tarduno et al., 2003; Wang et al., 2017). The relative motions between hot spots on adjacent plates have been investigated using kinematic models, but the results suffer from uncertainties in plate velocities and the ages of volcanic islands (Koivisto et al., 2014). Whereas Morgan (1983), Morgan and Morgan (2007), and Duncan (1981) suggested that individual hot spots move slowly relative to the average reference frame, with a speed of less than 5 mm/year in the past ~100 Ma, Molnar and Stock (1987) showed that the Hawaiian hot spot moved as fast as 10–20 mm/year for the last ~50–65 Ma relative to the Indo-Atlantic hot spots. Using updated plate circuit reconstructions, Koivisto et al. (2014) showed that the average relative motions between the Indo-Atlantic hot spots and the Pacific hot spots are as low as 2–6 mm/year in the past 48 Ma, but with large uncertainties (about ±6 mm/year).

More recently, Wang et al. (2017) computed lateral motions of 56 observed hot spots in the direction perpendicular to hot spot tracks (V_{perp}) in the last 5 Ma, based on the relative plate velocities and the trend of observed hot spot tracks (Morgan & Morgan, 2007). They found that the V_{perp} of individual hot spots ranges from 0 to 34.6 mm/year, but the global mean value of V_{perp} is as small as 3.2 ± 2.7 mm/year. However, this study did not constrain the lateral motion of hot spots prior to 5 Ma and that parallel to the hot spot tracks.

Additional constraints on the lateral motion of hot spots come from paleomagnetism. For example, rapid southward motion (>40 mm/year) of the Hawaiian hot spot during the period of 81–47 Ma has been suggested by Tarduno et al. (2003) based on paleomagnetic data. However, paleomagnetic data only provide information about the paleolatitudes of hot spots. It is also unclear how much the latitudinal changes of hot spots are due to true polar wander (Besse & Courtillot, 2002).

It is generally accepted that at least some hot spots are caused by mantle plumes (e.g., Courtillot et al., 2003). The rise of mantle plumes from the basal thermal boundary layer to beneath the lithosphere is inevitably affected by the surrounding mantle flow. The lateral motions of mantle plumes have been studied by Steinberger et al. (Steinberger, 2000; Steinberger & Antretter, 2006; Steinberger & O'Connell, 1998). However, their results suffer from uncertainties of mantle density and viscosity based on which the background mantle flow is computed. Their models also assume that the initial plume conduits are vertical without deflection, but this assumption has not been justified. In addition, as suggested by Kerr and Lister (2008) through lab experiments, the plume rise velocity at different mantle depths used by Steinberger and O'Connell (1998) and Steinberger (2000) needs to be corrected by a factor of 0.8–14.3, and the plume rise velocity used in the models of Steinberger and Antretter (2006) is overestimated by about 50%.

The lateral motions of plumes were also investigated in laboratory studies (e.g., Kerr & Lister, 2008; Richards & Griffiths, 1988) and in 3-D global mantle convection models with dynamically generated plumes and plates (e.g., Zhong et al., 2000). Particularly, Zhong et al. (2000) found that mantle plumes would form in flow stagnation regions at the core-mantle boundary (CMB) and move laterally at an average speed that ranges from 1/3 to 1/5 of the surface plate motions, from shallow to large depths in the mantle. Recently, Hassan et al. (2016) performed global mantle convection models with imposed plate motion history on the surface. They suggested that the Hawaiian plume moved ~10° southward between 81 and 47 Ma with an average speed of ~32.7 mm/year, and the lateral plume motion decreased to ~9 mm/year between 47 Ma and the present day.

Here, we quantify the lateral motion of all long-lived plumes in 3-D full spherical mantle convection models. The locations of plumes in convection models are model dependent, and they are rarely located at the precise locations of observed hot spots (Hassan et al., 2015; Li & Zhong, 2017). We thus focus on the statistics of the lateral motions of plumes, rather than the motion of individual hot spots. We notice that the terms "plume" and "hot spot" are sometimes used interchangeably. For clarity, we use plume to refer to a hot thermal structure in geodynamic models, and hot spot refers to a true melting area beneath the surface that produce active volcanoes.

2. Methods

The setup of the 3-D convection models is similar to Li and Zhong (2017). The models have a dimensionless radius of 0.55 and 1.0 at the CMB and the surface, respectively. The computational domain is divided into 12 caps with each cap containing $256 \times 256 \times 80$ elements, leading to a lateral resolution of ~15 and ~25 km at the CMB and the surface, respectively. The grids are refined radially in the lowermost ~200 km of the mantle to a radial resolution of ~24 km. Plumes are resolved at all depths in our very high resolution models, including in the upper mantle where plumes have relatively small radius (Figure S1 in the supporting information). The equations of the conservation of mass, momentum, and energy are solved under the Boussinesq approximation using CitcomS (Zhong et al., 2008).

The temperature is fixed at $T = 0$ and 1 on the surface and the CMB, respectively. Models are both basally and internally heated, with a nondimensional internal heating rate of $Q = 100$ (or $\sim 6 \times 10^{-12}$ W/kg), leading to ~50–70% of internal heating ratio. Reference values of physical parameters used for nondimensionalization are provided in Table S1. We impose plate motion history at the surface back to 458 Ma (Seton et al., 2012; Zhang et al., 2010), while the CMB is free slip. The initial (nondimensional) temperature is a 1-D profile that increases linearly from 0 at the surface to 0.558 for depths deeper than 275 km.

The viscosity is both temperature and depth dependent, expressed as $\eta = \eta_0 \exp[A(0.5 - T)]$, where the activation coefficient A is 9.21 for most cases (e.g., equivalent to ~190 kJ/mol of activation energy), leading to a maximum of 4 orders viscosity change due to variation of temperature. The activation energy of temperature-dependent viscosity is not well constrained, which depends on the water content and the

Table 1
Cases Used in This Study

Case	*Ra*	*A*	*B*	Thermochemical
1	1×10^8	9.21	N/A	No
2	2×10^8	9.21	N/A	No
3	5×10^7	9.21	N/A	No
4	2×10^8	11.51	N/A	No
5	1×10^8	9.21	0.22	Yes

Note. Ra = Rayleigh number; A = activation coefficient for temperature dependence of viscosity; B = buoyancy number.

mechanism of creep (e.g., Karato & Wu, 1993). We thus test the effects of different activation coefficient. The η_0 determines the depth dependence of viscosity, with η_0 = 1.0 and 1/30 in the uppermost 150 and 150- to 670-km depths, respectively. We employ a 60 times viscosity increase at the 670-km depth into the lower mantle, and there is a factor of ~3.4 linear viscosity increases from 670 km to the CMB. Our models also include a linear increase of thermal diffusivity and decrease of thermal expansivity from the surface to the CMB by a factor of 2.18 and 3.0, respectively, as suggested by mineral physics studies (e.g., Hsieh et al., 2018; Tackley, 2012).

Plumes are defined in regions where (1) the residual temperature (e.g., after the horizontal average temperature is removed) is larger than 0.04 (or 100 K if scaled with a reference temperature of ΔT = 2500 K) and (2) the radial velocity is positive (or upward). In addition, we only define plumes in regions where hot conduits that satisfy conditions (1) and (2) also extend continuously from 2,000-km depth to at least 330-km depth. If two or more plumes are within 3° from one another, they are treated as one plume. Although our calculations start from 458 Ma, we focus on the lateral motion of mantle plumes in the last 80 Ma, because (1) the uncertainty of plate motion history increases back in time, (2) we want to avoid the effects of initial condition, and (3) 80 Ma is close to the maximum age of the ancient island volcanoes observed on the Earth that are associated with a hot spot track.

We compute the locations of hot spot tracks from the locations of plumes and plate motion history in the past 80 Ma (Seton et al., 2012). New "virtual" volcanos are initially produced at locations directly above plumes at each time. After formed, the virtual volcanos are advected away from their initial locations by plate motion. During these processes, imaginary chains of virtual volcanos or virtual hot spot tracks form on the surface.

3. Results

We first show the results for the case 1 (Table 1), which is an isochemical model with a Rayleigh number of $Ra = 1\times10^8$ and an activation coefficient of A = 9.21. Figures 1a–1e show the lateral mantle flow velocities at the surface and 330-, 700-, and 1,450-km depths, respectively, together with plume trajectories at 330-km depth for the last 80 Ma. We find that the plume trajectories are generally different from the directions of plate motion and the upper mantle lateral flow. For example, many of the plumes in the central Pacific and the North Africa are moving subperpendicular to the plate motion and the upper mantle lateral flow, and plumes in the southeast Africa are moving in the opposite directions of the plate motion and the upper mantle lateral flow (Figures 1a and 1b). In contrast, the plume trajectories are largely consistent with the lateral flow in the lower mantle (Figures 1c–1e), which may indicate that the lateral motions of mantle plumes are significantly controlled by mantle flows in the lower mantle. The dramatic changes of mantle flow velocities from the upper mantle (Figure 1b) to the lower mantle (Figures 1c–1e) may be caused by the sixtyfold viscosity increase across the 670-km depth seismic discontinuity into the lower mantle.

Most inferred hot spot tracks have a linear shape (Figure 1f), and their lengths vary from place to place, which are mainly controlled by the speed of plate motion. Some hot spot tracks on the north Pacific show a bending at around 40 Ma (similar to the Hawaiian-Emperor hot spot tracks on the Earth), which is caused by the changes of plate motion direction around this time.

We compute the average velocity of the lateral motion of mantle plumes at 330-km depth within 4 time intervals: 80–60, 60–40, 40–20, and from 20 to 0 Ma (e.g., present day). Within each 20-Myr time interval, only the lateral motions of long-lived plumes that last for more than 15 Myr are quantified. As shown in Figure 2a, the plume lateral motions generally decrease from ~10–40 mm/year during 80–60 and 60–40 Ma, to ~5-30 mm/year during 40–20 Ma, and to ~0–25 mm/year during 20–0 Ma. The plate motions in a hot spot reference frame often have significant net rotation for the present day and the past (e.g., Gordon & Jurdy, 1986; Seton et al., 2012). When suitable lateral variations of viscosity in the lithosphere are included, the sublithospheric mantle would display net rotation that has significantly smaller rate than that for the lithosphere but counterbalances the lithospheric net rotation (Rudolph & Zhong, 2014; Zhong, 2001). However, in our models, the mantle has similar net rotation to the lithospheric net rotation because of simplified mantle viscosity. We find that the average angular velocity for the net rotation at 330-km depth decreases from ~0.32°/Myr

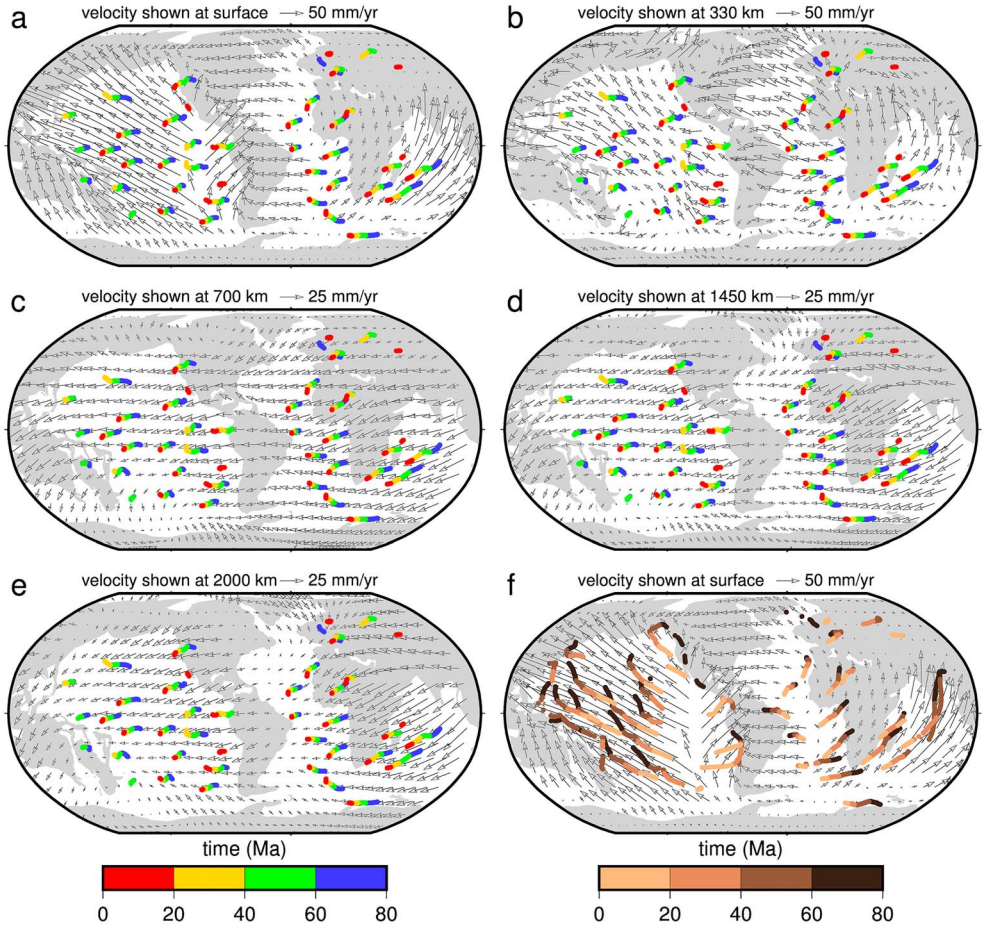

Figure 1. Plume trajectories at 330-km depth (a–e) and inferred hot spot tracks (f) for case 1. The arrows in (a)–(f) show the time averaged lateral motion of mantle flow velocity in the past 80 Ma at the surface (a, f) and at depths of 330 km (b), 700 km (c), 1,450 km (d), and 2,000 km (e). The net rotation of mantle flows is included in all figure panels. The continents (gray) are shown at the present day.

during 40–80 Ma, to ~0.16°/Myr during 40–20 Ma, and to ~0.08°/Myr during 20–0 Ma (Figure S2), which may cause the relatively large plume lateral motions during 80–40 Ma and the time-dependent characteristics of the plume lateral motions in the last 80 Ma (Figure 2a). Hereafter, the lateral motions of plumes presented have the net rotation components removed; therefore, they can be viewed as in a no-net-rotation frame.

The lateral motions of plumes are significantly reduced after the net rotation component is removed, and they become less time dependent (Figure 2b). Ninety-seven percent of plumes move laterally with a speed less than 20 mm/year. In addition, the speeds of plume motions perpendicular (Figure 2c) to the inferred hot spot tracks (Figure 1f) are statistically similar to that parallel (Figure 2d) to the inferred hot spot tracks, both with a speed of less than 20 mm/year for almost all plumes in the last 80 Ma. To compare with the study of Wang et al. (2017), we project the lateral motion of mantle plumes to the direction perpendicular to the inferred hot spot tracks in the last 5 Ma. Our results are statistically the same as that of Wang et al. (2017; Figures 2e and 2f). In both studies, the lateral motions of mantle plumes are much smaller than the speeds of the plates above the plumes, and there is no clear correlation between the two (Figure 2f).

Figures 3a–3d show the lateral motions of individual plumes at 330-km depth in the last 80 Ma for case 1. We find that more than half of mantle plumes in the Pacific move coherently in the southeastern directions during 80–60 Ma (Figure 3a), 40–20 Ma (Figure 3c), and 20–0 Ma (Figure 3d) and move coherently eastward during 60–40 Ma (Figure 3b). The northward and westward motions of plumes mainly locate at the East and the South Pacific (Figures 3b–3d). The lateral motions of the Indo-Atlantic plumes vary more

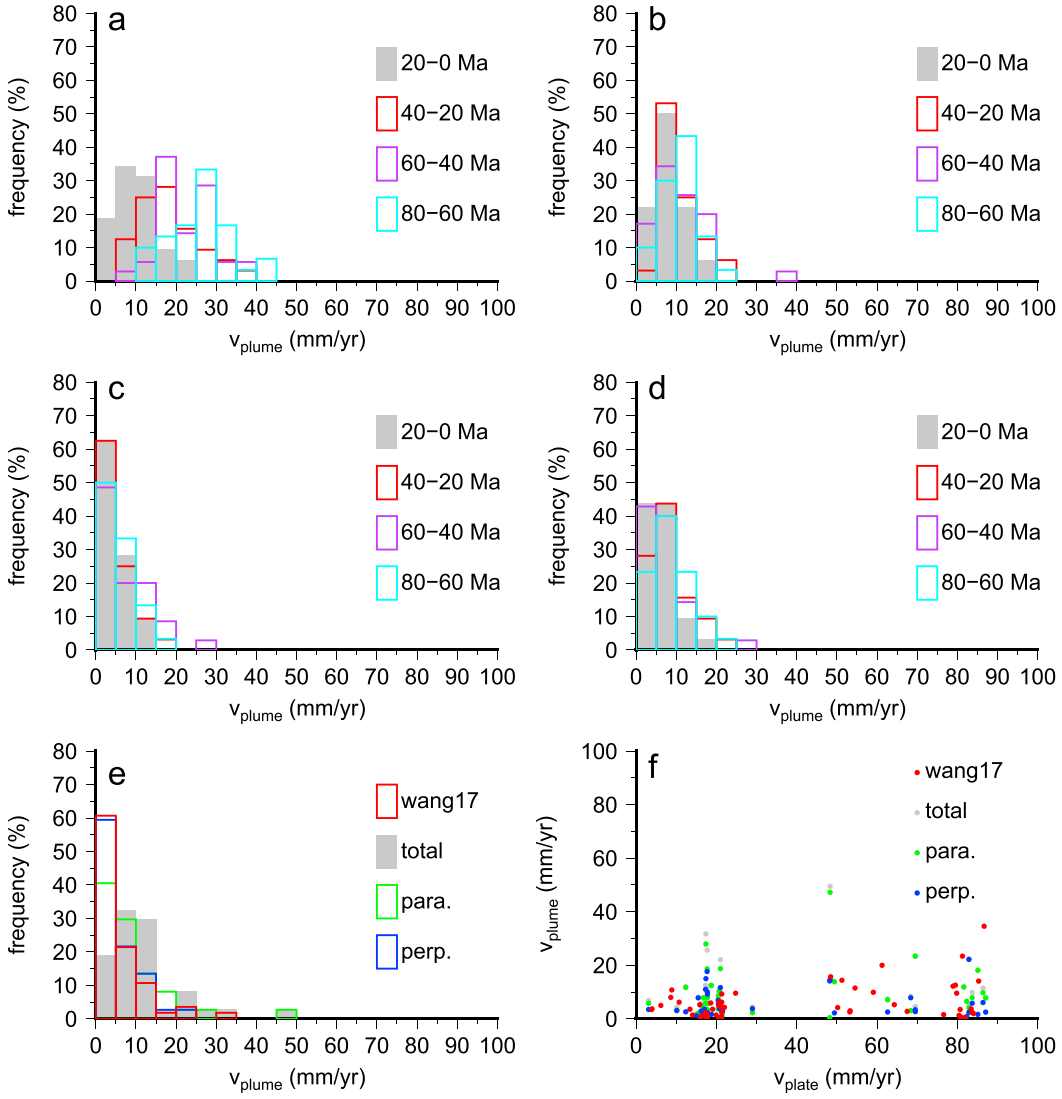

Figure 2. The lateral motion of plumes at 330-km depth in the last 80 Ma for case 1 and their comparison with observations. (a–d) Histograms of the average lateral motion of plumes within 4 time intervals of 80–60, 60–40, 40–20, and 20–0 Ma. (e–f) Average lateral motion of plumes in the past 5 Ma, compared with the lateral motions of observed hot spots computed by Wang et al., (2017) and the surface plate velocity above the plumes or observed hot spots (f). The net rotation component of plume motions is removed in panels (b)–(f) and is included in panel (a). Panels (c) and (d), respectively, show the plume motion in the directions perpendicular and parallel to the inferred hot spot tracks (Figure 1f).

significantly from place to place and do not show clear coherent motions. However, the speeds of the lateral motions of the Pacific plumes are statistically similar to the Indo-Atlantic plumes (Figures 3e–3h).

Additional cases are performed to explore the effects of model parameters on the results (Table 1). In cases 2 and 3, the Rayleigh numbers are increased to $Ra = 2 \times 10^8$ and decreased to $Ra = 5 \times 10^7$, respectively, whereas other parameters are the same as case 1. Case 4 has a larger activation coefficient of $A = 11.51$ (e.g., equivalent to an activation energy of ~240 kJ/mol) for the temperature-dependent viscosity, which leads to a maximum of 5 orders viscosity change, and is restarted from case 2 at 200 Ma to speed up the calculation. Case 5 is a thermochemical calculation (e.g., Hassan et al., 2016; Li & Zhong, 2017; Zhang et al., 2010) in which we initially introduce a global layer of compositionally dense materials in the lowermost 200 km of the mantle, with a buoyancy number of $B = 0.22$, which is defined as the ratio between intrinsic density anomaly and density anomaly due to thermal expansion, or $B = \Delta\rho/\rho_0\alpha_0\Delta T$ with $\Delta\rho$ the intrinsic density anomaly, ρ_0 and α_0 the reference density and thermal expansivity, respectively, and ΔT the

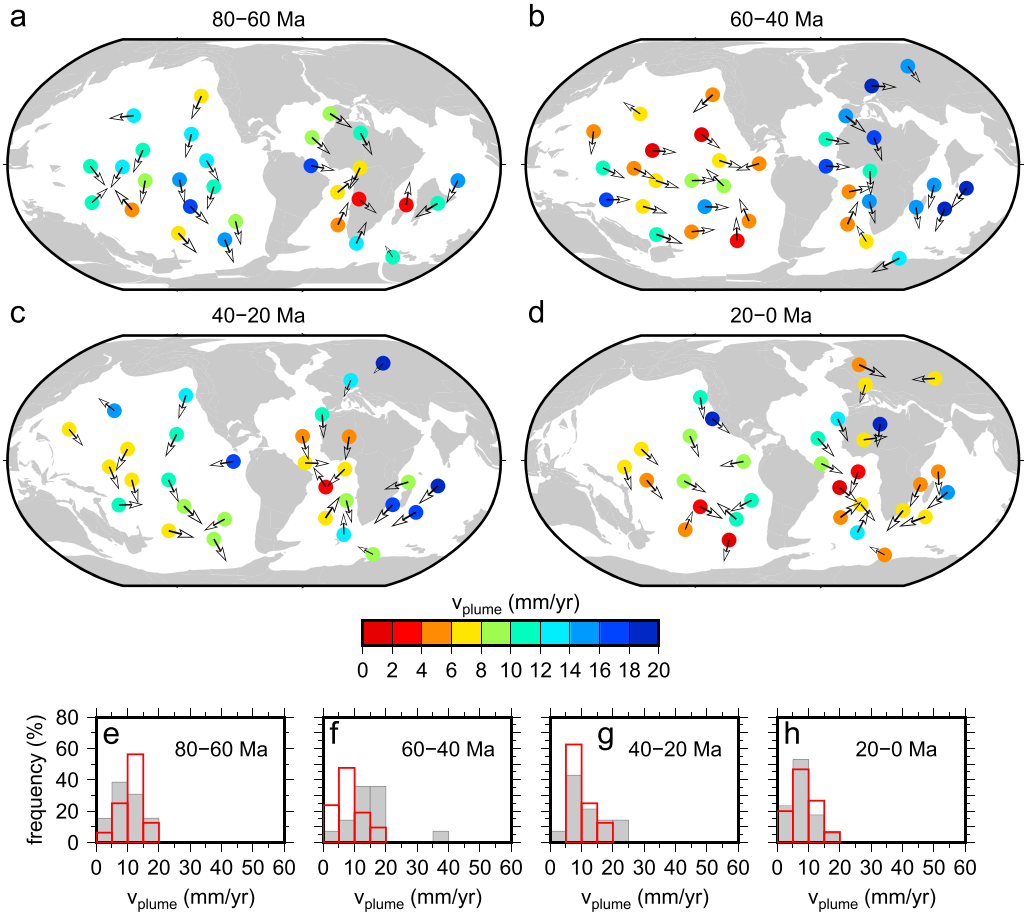

Figure 3. The distribution and lateral motion of plumes at 330-km depth for case 1. (a–d) Speed (represented by colored circles) and direction (represented by arrows) of the lateral motion of plumes during 80–60 Ma (a), 60–40 Ma (b), 40–20 Ma (c), and 20–0 Ma (d). The continents (gray) are shown at 70 Ma (a), 50 Ma (b), 30 Ma (c), and 10 Ma (d). (e–h) Lateral motions of plumes beneath the Pacific (red) and the Indo-Atlantic (gray) during 80–60 Ma (e), 60–40 Ma (f), 40–20 Ma (g), and 20–0 Ma (h). The net rotation in plume lateral motions is removed.

reference temperature. The advection of the compositional field is simulated with ~1.26 billion tracers using the ratio tracer method (Tackley & King, 2003).

The number of long-lived plumes, which last for at least 15 Myr within each 20-Myr period, varies from case to case, with 29–35 plumes in case 1 (Figure 3), 39–47 plumes in case 2 (Figure S3), 9–16 plumes in case 3 (Figure S4), 44–52 plumes in case 4 (Figure S5), and 16–24 plumes in case 5 (Figure S6). In general, the radius of plumes increases with decreasing Rayleigh number but decreases with the degree of temperature dependent of viscosity. The intrinsically dense materials in case 5 are pushed into thermochemical piles beneath the Pacific and the Africa at present day, with most plumes occurring above the piles and many of them near the pile edges (Figure S6).

As shown in Figure 4a, the precise locations of mantle plumes are model dependent. There are times when plumes in different models happen to occur at close locations, but the direction and magnitude of the lateral motions of these plumes change from one to another. Nevertheless, the lateral motions of plumes are statistically similar in all models (Figures 4b–4e). The majority (>90%) of plumes move laterally with a speed in the range of 0–20 mm/year in the last 80 Ma (Figures 4b–4e). During this time period, ~10–20% of mantle plumes move laterally with a speed less than 5 mm/year, and ~40–60% plumes have a speed less than 10 mm/year.

For comparison, we also quantify the lateral motions of plumes in case 1 at 700-km depth. As shown in Figures S7 and S8, most plumes have similar lateral motion at different depths. However, plumes with

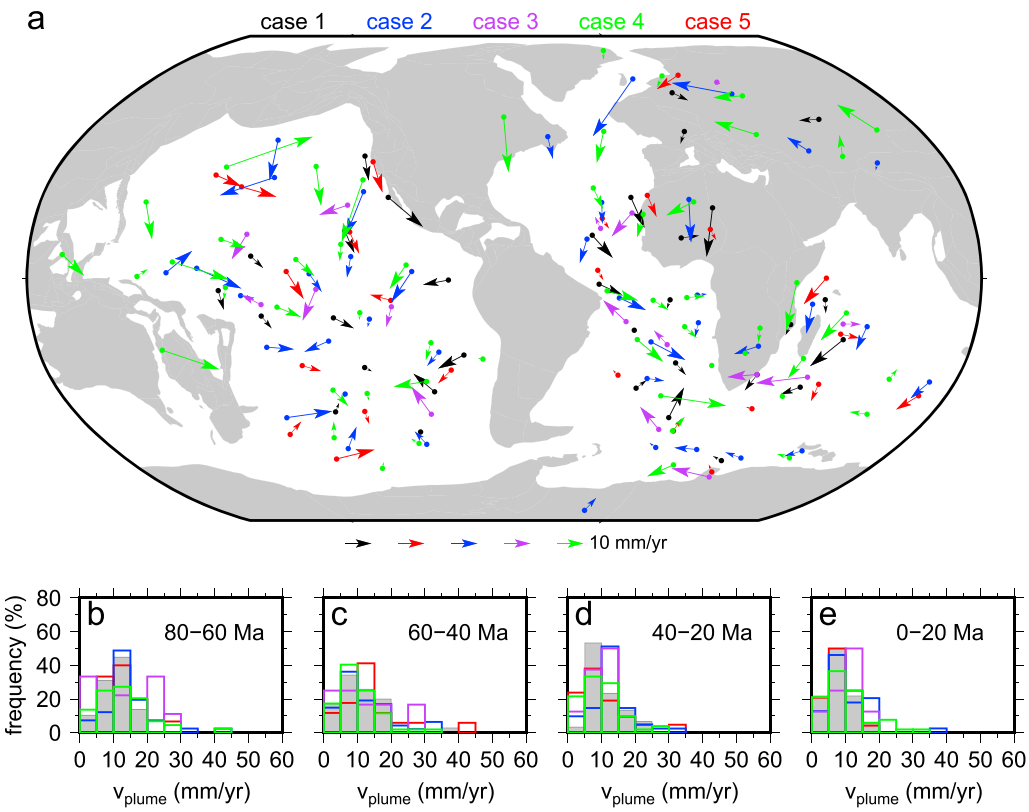

Figure 4. The lateral motion of plumes at 330-km depth for all five cases. (a) The average lateral velocity of plumes in the past 20 Ma for case 1 (black), case 2 (blue), case 3 (purple), case 4 (green), and case 5 (red). (b–e) Average lateral motion of long-lived plumes during time intervals of 80–60 Ma (b), 60–40 Ma (c), 40–20 Ma (d), and 20–0 Ma (e) for case 1 (gray), case 2 (blue), case 3 (purple), case 4 (green), and case 5 (red). The plume lateral motions in (a)–(e) have their net rotation component removed. The continents (gray) are shown at present day. The Rayleigh number for case 1, case 2, and case 3 are 1×10^8, 2×10^8, and 5×10^7, respectively. Case 4 has $A = 11.51$, and case 5 is thermochemical.

significant different lateral motions at different depths are also observed, which would lead to tilting of the plume conduits (Hassan et al., 2016). Nevertheless, the statistics of plume lateral motions are the same for different depths.

4. Discussion

Here, we quantify the lateral motion of mantle plumes in 3-D global mantle convection models using very high model resolution (<25 km laterally). Plate motion history is employed to guide the large-scale convection pattern; therefore, the large-scale mantle flow in our models, which may play a significant role on the lateral motion of plumes, is consistent with plate motion history. In addition, plumes form naturally as a result of thermal boundary layer instabilities, and the dynamics of mantle plumes is self-consistent with the global mantle flow. Our results are supported by the statistical consistence with the lateral motion of hot spots based on kinematic models (Wang et al., 2017).

Previous studies have suggested a lateral motion of hot spots ranging from almost no motion (<5 mm/year; Duncan, 1981; Koivisto et al., 2014; Morgan, 1983; Morgan & Morgan, 2007; Müller et al., 1993) to moderate motion (~10–20 mm/year; Molnar & Stock, 1987), and to motions larger than ~20 mm/year (Hassan et al., 2016; Raymond et al., 2000; Tarduno et al., 2003) in the past ~100 Ma. A small-to-moderate (~2–12 mm/year) lateral motion of hot spots under the no-net-rotation reference frame in the past ~70 Ma has been suggested by Steinberger and O'Connell (1998). Here, we show that the majority of plumes (>90%) move laterally with a speed of 0–20 mm/year in the upper mantle (e.g., Figures 2b and 4b–4e). A small number of plumes (<10%) that move faster than 20 mm/year are also observed. Our results suggest a small to

moderate lateral motion for most plume-caused hot spots. It would be quite uncommon, though not impossible, for hot spots to move laterally with a speed larger than 20 mm/year.

Using the analysis of empirical age progressions for hot spot tracks on the Pacific plate, Wessel and Kroenke (2009) suggested that there is coherent southward motion between the Hawaii and Louisville hot spots during 80–55 Ma. In our models, the imposed plate motion in the last 200 Ma (Seton et al., 2012) has an intrinsic lithospheric net rotation component in the approximately west direction, which causes a westward net rotation of the deep mantle. This explains why plumes move coherently in the west direction (Figures 1a–1e). After the net rotation of the mantle flow is removed, there is no coherent lateral motion of mantle plumes on a global scale (Figures 3a–3d). However, coherent plume motion sometimes exists locally. For example, >50% of plumes in the Pacific move approximately southward in all cases during 80–60 Ma (Figures 3 and S3–S6), consistent with the studies of Wessel and Kroenke (2009). Our results suggest that coherent motions among a group of hot spots are possible, particularly for hot spots in nearby regions; however, to what extent the hot spots move coherently on a global scale depends on the large-scale mantle flow.

The statistics of plume lateral motions do not change significantly in cases with increased activation coefficient A of the temperature-dependent viscosity (case 4), nor with different Rayleigh number (cases 1, 3, and 4; Figures 4b–4e), nor with the presence of thermochemical piles in the lowermost mantle (case 5). This may be because all cases have the same imposed plate motion history and thus similar large-scale convection patterns. Nevertheless, although the plume lateral motions are statistically similar in all models, the number and locations of individual plumes are rather model dependent (e.g., Figure 4a) due to the nature of thermal boundary layer instabilities (Li & Zhong, 2017; Olson, 1993). Even though plumes in different models sometimes occur at close locations, their lateral motions can be very different (e.g., Figure 4a). Therefore, care needs to be exercised when relating lateral motions of individual plumes in convection models to observed hot spots.

5. Conclusion

In summary, we perform 3-D very high resolution (<25 km laterally), full spherical, global mantle convection models with realistic convection vigor to examine the lateral motion of plumes in the upper mantle (i.e., 330-km depth). We find that the lateral motions of individual plumes vary from place to place and are model dependent, but coherent plume motions are found in local regions, for example, with more than 50% of plumes in the Pacific moving coherently southward during 80–60 Ma. The lateral motions of Pacific plumes are statistically similar to the Indo-Atlantic plumes. Greater than 90% of plumes move laterally with a speed less than 20 mm/year in the past 80 Ma, under the no-net-rotation reference frame. Only a relatively small portion of plumes (~10–20%) move laterally at less than 5 mm/year. The statistics of plume lateral motions in the last 5 Ma agrees with the lateral motion of observed hot spots determined in kinematic models.

Acknowledgments
We thank two anonymous reviewers and Editor Jeroen Ritsema for their constructive comments. This work is supported by National Science Foundation through Grants 1135382 and 1645245. M. L. is also supported by Arizona State University through startup funding. This work used the Agave cluster at Arizona State University, the Yellowstone cluster provided by NCAR's Computational and Information Systems Laboratory sponsored by the National Science Foundation, and the Extreme Science and Engineering Discovery Environment (XSEDE) resource-name at the service-provider through allocation *mingming*. The mantle convection code CitcomS is available at the website (https://geodynamics.org/cig/software/citcoms/).

References

Besse, J., & Courtillot, V. (2002). Apparent and true polar wander and the geometry of the geomagnetic field over the last 200 Myr. *Journal of Geophysical Research*, *107*(B11), 2300. https://doi.org/10.1029/2000JB000050

Courtillot, V., Davaille, A., Besse, J., & Stock, J. (2003). Three distinct types of hotspots in the Earth's mantle. *Earth and Planetary Science Letters*, *205*(3-4), 295–308. https://doi.org/10.1016/S0012-821x(02)01048-8

Duncan, R. A. (1981). Hotspots in the Southern Oceans—An absolute frame of reference for motion of the Gondwana continents. *Tectonophysics*, *74*, 29–42. https://doi.org/10.1016/0040-1951(81)90126-8

Duncan, R. A., & Richards, M. A. (1991). Hotspots, mantle plumes, flood basalts, and true polar wander. *Reviews of Geophysics*, *29*, 31–50. https://doi.org/10.1029/90RG02372

Gordon, R. G., & Cape, C. D. (1981). Cenozoic latitudinal shift of the Hawaiian hotspot and its implications for true polar wander. *Earth and Planetary Science Letters*, *55*, 37–47. https://doi.org/10.1016/0012-821x(81)90084-4

Gordon, R. G., & Jurdy, D. (1986). Cenozoic global plate motions. *Journal of Geophysical Research*, *91*, 12389–12406. https://doi.org/10.1029/JB091iB12p12389

Hassan, R., Flament, N., Gurnis, M., Bower, D. J., & Müller, D. (2015). Provenance of plumes in global convection models. *Geochemistry, Geophysics, Geosystems*, 1465–1489. https://doi.org/10.1002/2015GC005751

Hassan, R., Müller, R. D., Gurnis, M., Williams, S. E., & Flament, N. (2016). A rapid burst in hotspot motion through the interaction of tectonics and deep mantle flow. *Nature*, *533*, 239–242. https://doi.org/10.1038/nature17422

Hsieh, W.-P., Deschamps, F., Okuchi, T., & Lin, J.-F. (2018). Effects of iron on the lattice thermal conductivity of Earth's deep mantle and implications for mantle dynamics. *Proceedings of the National Academy of Sciences*. https://doi.org/10.1073/pnas.1718557115

Karato, S., & Wu, P. (1993). Rheology of the upper mantle—A synthesis. *Science*, *260*, 771–778.

Kerr, R. C., & Lister, J. R. (2008). Rise and deflection of mantle plume tails. *Geochemistry, Geophysics, Geosystems*, *9*, Q10004. https://doi.org/10.1029/2008GC002124

Koivisto, E. A., Andrews, D. L., & Gordon, R. G. (2014). Tests of fixity of the Indo-Atlantic hot spots relative to Pacific hot spots. *Journal of Geophysical Research: Solid Earth*, *119*, 661–675. https://doi.org/10.1002/2013JB010413

Li, M., & Zhong, S. (2017). The source location of mantle plumes from 3D spherical models of mantle convection. *Earth and Planetary Science Letters*, *478*, 47–57. https://doi.org/10.1016/j.epsl.2017.08.033

Molnar, P., & Stock, J. (1987). Relative motions of hotspots in the Pacific, Atlantic and Indian Oceans since late Cretaceous time. *Nature*, *327*, 587–591. https://doi.org/10.1038/327587a0

Morgan, W. J. (1972). Plate Motions and Deep Mantle Convection. In R. Shagam, R. B. Hargraves, W. J. Morgan, F. B. van Houten, C. A. Burk, H. D. Holland, & L. C. Hollister (Eds.), *Studies in Earth and Space Sciences*. Geological Society of America, 132, 7–22. https://doi.org/10.1130/MEM132-p7

Morgan, W. J. (1983). Hotspot tracks and the early rifting of the Atlantic. *Tectonophysics*, *94*, 123–139. https://doi.org/10.1016/0040-1951(83)90013-6

Morgan, W.J., & Morgan, J.P. (2007). Plate velocities in the hotspot reference frame. 430, 65-78. https://doi.org/10.1130/2007.2430(04)

Müller, R. D., Royer, J. Y., & Lawver, L. A. (1993). Revised plate motions relative to the hotspots from combined Atlantic and Indian-Ocean hotspot tracks. *Geology*, *21*, 275–278. https://doi.org/10.1130/0091-7613(1993)021<0275:Rpmrtt>2.3.Co;2

Olson, P. (1993). Hot spots, swells and mantle plumes. In M. P. Ryan (Ed.), *Magma transport and storage*. New York: John Wiley, 33–51.

Raymond, C.A., Stock, J.M., & Cande, S.C. (2000). Fast paleogene motion of the pacific hotspots from revised global plate circuit constraints, The history and dynamics of global plate motions, pp. 359-375.

Richards, M. A., & Griffiths, R. W. (1988). Deflection of plumes by mantle shear flow: Experimental results and a simple theory. *Geophysical Journal International*, *94*, 367–376. https://doi.org/10.1111/j.1365-246X.1988.tb02260.x

Rudolph, M. L., & Zhong, S. J. (2014). History and dynamics of net rotation of the mantle and lithosphere. *Geochemistry, Geophysics, Geosystems*, *15*, 3645–3657. https://doi.org/10.1002/2014GC005457

Seton, M., Müller, R. D., Zahirovic, S., Gaina, C., Torsvik, T., Shephard, G., et al. (2012). Global continental and ocean basin reconstructions since 200 Ma. *Earth-Science Reviews*, *113*, 212–270. https://doi.org/10.1016/j.earscirev.2012.03.002

Steinberger, B. (2000). Plumes in a convecting mantle: Models and observations for individual hotspots. *Journal of Geophysical Research*, *105*, 11,127–11,152. https://doi.org/10.1029/1999JB900398

Steinberger, B., & Antretter, M. (2006). Conduit diameter and buoyant rising speed of mantle plumes: Implications for the motion of hot spots and shape of plume conduits. *Geochemistry, Geophysics, Geosystems*, *7*, Q11018. https://doi.org/10.1029/2006GC001409

Steinberger, B., & O'Connell, R. J. (1998). Advection of plumes in mantle flow: implications for hotspot motion, mantle viscosity and plume distribution. *Geophysical Journal International*, *132*, 412–434. https://doi.org/10.1046/j.1365-246x.1998.00447.x

Tackley, P. J. (2012). Dynamics and evolution of the deep mantle resulting from thermal, chemical, phase and melting effects. *Earth-Science Reviews*, *110*, 1–25. https://doi.org/10.1016/j.earscirev.2011.10.001

Tackley, P. J., & King, S. D. (2003). Testing the tracer ratio method for modeling active compositional fields in mantle convection simulations. *Geochemistry, Geophysics, Geosystems*, *4*(4), 8302. https://doi.org/10.1029/2001GC000214

Tarduno, J. A., Duncan, R. A., Scholl, D. W., Cottrell, R. D., Steinberger, B., Thordarson, T., et al. (2003). The Emperor Seamounts: Southward motion of the Hawaiian hotspot plume in earth's mantle. *Science*, *301*, 1064–1069. https://doi.org/10.1126/science.1086442

Wang, C. Z., Gordon, R. G., & Zhang, T. (2017). Bounds on geologically current rates of motion of groups of hot spots. *Geophysical Research Letters*, *44*, 6048–6056. https://doi.org/10.1002/2017GL073430

Wessel, P., & Kroenke, L. W. (2009). Observations of geometry and ages constrain relative motion of Hawaii and Louisville plumes. *Earth and Planetary Science Letters*, *284*(3-4), 467–472. https://doi.org/10.1016/j.epsl.2009.05.012

Wilson, J. T. (1963). A possible origin of the Hawaiian Islands. *Canadian Journal of Physics*, *41*, 863–870.

Zhang, N., Zhong, S., Leng, W., & Li, Z.-X. (2010). A model for the evolution of the Earth's mantle structure since the Early Paleozoic. *Journal of Geophysical Research*, *115*, B06401. https://doi.org/10.1029/2009JB006896

Zhong, S. J. (2001). Role of ocean-continent contrast and continental keels on Plate motion, net rotation of lithosphere and the geoid. *Journal of Geophysical Research*, *106*, 703–712. https://doi.org/10.1029/2000JB900364

Zhong, S. J., McNamara, A., Tan, E., Moresi, L., & Gurnis, M. (2008). A benchmark study on mantle convection in a 3-D spherical shell using CitcomS. *Geochemistry, Geophysics, Geosystems*, *9*, Q10017. https://doi.org/10.1029/2008GC002048

Zhong, S. J., Zuber, M. T., Moresi, L., & Gurnis, M. (2000). Role of temperature-dependent viscosity and surface plates in spherical shell models of mantle convection. *Journal of Geophysical Research*, *105*, 11,063–11,082. https://doi.org/10.1029/2000JB900003